LAWRENCE
LIVERMORE
NATIONAL
LABORATORY

UCRL-TR-218576

A comparison of dispersion calculations in bluff body wakes using LES and unsteady RANS

J.S. Paschkewitz

February 1, 2006

This work was performed under the auspices of the U.S. Department of Energy by University of California, Lawrence Livermore National Laboratory under Contract W-7405-Eng-48.

A comparison of dispersion calculations in bluff body wakes using LES and unsteady RANS

By JOHN S. PASCHKEWITZ

Energy and Environment Directorate, Lawrence Livermore National Laboratory, Livermore, CA, 94551

19 January 2006

Accurate modeling of the dispersion behavior of sprays or particles is critical for a variety of problems including combustion, urban pollution or release events, and splash and spray transport around heavy vehicles. Bluff body wakes are particularly challenging since these flows are both highly separated and strongly unsteady. Attempting to model the dispersion of droplets or particles interacting with bluff body wakes is even more difficult since small differences in the flow field encountered by particles can lead to large differences in the dispersion behavior. Particles with finite inertia can exhibit additional complicating effects such as preferential concentration. In this preliminary study, we consider the dispersion of solid particles in the wake of a rectangular plane at a Reynolds number (Re) of 10000 and that of droplets in the wake of a simplified tractor-trailer geometry at $Re = 2 \times 10^6$ using both the Large Eddy Simulation (LES) and Unsteady Reynolds-Averaged Navier-Stokes (URANS) turbulence modeling approaches. The calculations were performed using identical meshes for both the LES and URANS models. Particle stresses are not backcoupled to the carrier fluid velocity solution. In the case of the rectangular plane wake, the LES calculation predicts a finer-scale and more persistent wake structure than the URANS one; the resulting particle dispersion is considerably ($\approx 40\%$) underpredicted for low inertia particles. For the case of the simplified tractor-trailer geometry, although the LES is underresolved, similar trends are observed with strong differences in the vertical and horizontal dispersion of the smallest particles. These results suggest that it may be necessary to use LES to accurately capture the dispersion behavior of small, low inertia particles or droplets, but that URANS may be sufficient for problems in which only large particles with substantial inertia are of primary concern.

1. Introduction

Particle dispersion and deposition are of interest in a large number of engineering applications including pollutant transport, engine sprays, and chemical reactors. In the case of the LLNL Heavy Vehicle Aerodynamics effort, water splash and spray around heavy vehicles is a frequently cited safety hazard that is strongly related to vehicle aerodynamics (Manser *et al.* 2003). One of the objectives of this effort has been to model and understand effective means of mitigating splash and spray through design guidance provided from computational fluid dynamics (CFD) simulations.

The heavy vehicle spray problem is particularly challenging since it involves the interaction of a spray with an unsteady bluff body wake. Modeling the wake alone is a

difficult task since the Reynolds-averaged Navier Stokes (RANS) modeling methodology predominant in engineering calculations has well-known shortcomings in accurately simulating this class of flows. For example, steady RANS models have been shown to poorly predict the flow features in a variety of "canonical" problems such as the surface-mounted cube (Rodi 1997), the surface hump (Krishnan *et al.* 2004), and the asymmetric two-dimensional diffuser (Iaccarino 2001), particularly when the popular $k-\epsilon$ turbulence model is employed. More accurate solution methodologies, such as unsteady RANS (Iaccarino *et al.* 2003) as well as more complex turbulence models such as $v^2 - f$ (Iaccarino 2001) and large eddy simulation (LES) (Rodi 1997) have been shown to improve the agreement between the experimental and computational data. The first objective of this study was to qualitatively compare the flow predictions obtained using two of these "improved" strategies- LES and unsteady RANS (URANS)- on multiple bluff body wake problems.

The second objective of this work was to compare the particle dispersion predicted using LES and URANS in bluff body wakes. As the particle transport is sensitive to the small-scale and time-dependent details of the flow field, the dispersion caculations are strongly affected by the turbulence model. The particle dispersion is especially sensitive to the details of the flow field when the particles have finite inertia.

Particle inertia is responsible for the "particle focusing" effect (Eaton & Fessler 1994) in which particles interact with coherent structures in the flow differently depending on their inertia. For example, in a vortex street, low inertia particles are concentrated in the vortex cores, moderate inertia particles along the edges, and high inertia particles act ballistically, ignoring the vortices entirely. The relevant non-dimensional parameter to characterize the particle inertia is the Stokes number (St), which is the ratio of the particle velocity response time scale, τ_v, to the flow time scale, τ_f:

$$St = \frac{\tau_v}{\tau_f} = \frac{\rho_p D^2/18\mu_c}{U/l} = \frac{\rho D^2 l}{18\mu_c U}, \tag{1.1}$$

where D is the particle diameter, ρ_p is the particle density, μ_c is the carrier fluid dynamic viscosity, U is a characteristic velocity and l is a characteristic length scale for the flow. Particle focusing effects are most pronounced for particles having Stokes numbers in the range 0.1 to 1 (Eaton & Fessler 1994). Large eddy simulation models have generally provided superior estimates of the particle dispersion in swirling and separated flows (Apte *et al.* 2003; Sommerfeld & Qiu 1993).

In this report, we present preliminary results of simulations of the dispersion of particles and sprays in bluff body wakes obtained using the commercial CFD code StarCD (cd adapco 2005). We compare particle dispersion predictions in two bluff body wakes using the LES and URANS turbulence models implemented in this code. The first is the three dimensional plane wake experimentally studied by Crowe and coworkers (Tang *et al.* 1992; Yang *et al.* 2000); this case clearly illustrates the phenomenon of preferential concentration. The second is the Ground Transportation System (GTS) model, which is a simplified model of a heavy vehicle. We consider the dispersion of particles in the first case and droplets in the second.

This report is organized as follows. The governing equations for the carrier gas and particles or droplets are presented in Section 2. Empirical relationships for the collision-induced breakup of droplets are also briefly discussed. In Section 3 the geometric definitions for the two bluff bodies and the simulation parameters are provided. In Section 4, we present flow field characterizations as well as dispersion measures for both of these cases and we conclude in Section 5.

2. Problem Formulation

2.1. *Governing equations for fluid flow*

The equations for the carrier fluid flow are solved using the URANS and LES methodologies. We begin with the URANS formulation; in this case the velocity field is decomposed into mean and fluctuating components Eq. 2.1; the resulting *ensemble-averaged* Navier-Stokes equations Eq. 2.2 contain an unknown Reynolds stress term that must be defined using a closure approximation.

$$u_i(x_k,t) = U_i(x_k) + u'(x_k,t) \tag{2.1}$$

$$\frac{DU_i}{Dt} = -\frac{1}{\rho}\frac{\partial P}{\partial x_i} + \frac{\partial}{\partial x_j}\left(\nu\frac{\partial U_i}{\partial x_j}\right) + \frac{\partial(\overline{-u_i'u_j'})}{\partial x_j} \tag{2.2}$$

In this work we use the Menter Shear Stress Transport (SST) turbulence model (Menter 1994) to model the Reynolds stresses. This model was chosen since it is implemented in StarCD and has been shown in previous heavy vehicle aerodynamics CFD studies (Salari *et al.* 2004) to be more accurate than the simple $k-\epsilon$ and $k-\omega$ models. This two-equation model is based on the Boussinesq hypothesis that the Reynolds stresses are proportional to the local rate of strain S_{ij}, with the proportionality being the eddy viscosity ν_T:

$$\overline{-u_i'u_j'} = 2\nu_T S_{ij} \tag{2.3}$$

The SST model relates the eddy viscosity to the turbulent kinetic energy k and the turbulence frequency ω:

$$\nu_T = C_\mu k/\omega \tag{2.4}$$

Transport equations are solved for both k and ω. By using a weighted average of the $k-\epsilon$ and $k-\omega$ models, with $k-\epsilon$ in the far-field and $k-\omega$ near the wall, the SST model obtains the superior behavior of the $k-\omega$ model near boundaries and for flows with streamwise pressure gradients. The model also avoids the strong sensitivity of the solution to the boundary value of ω at free-stream boundaries. The default values of the model constants in StarCD correspond to those in the work of Menter (1994).

For the LES simulations we used StarCD's large eddy simulation (LES) implementation. The LES model is based on a spatial filter of the velocity:

$$\overline{U_i}(\mathbf{x},t) = \int G(\mathbf{r},\mathbf{x})U_i(\mathbf{x}-\mathbf{r},t)d\mathbf{r}. \tag{2.5}$$

The exact form of the filter kernel $G(\mathbf{r},\mathbf{x})$ is not important within the context of the constant coefficient LES models used in StarCD as the application of the filter is never computed. The velocity can then be decomposed into resolved and sub-grid scale components:

$$u_i(x_k,t) = \overline{U_i}(x_k) + u'(x_k,t). \tag{2.6}$$

Inserting this definition into the Navier-Stokes equations, the filtered momentum equations are obtained:

$$\frac{\partial\overline{U_j}}{\partial t} + \frac{\partial\overline{U_i}(\overline{U_j})}{\partial x_i} = -\frac{1}{\rho}\frac{\partial\overline{P}}{\partial x_i} + \nu\frac{\partial^2\overline{U_j}}{\partial x_i\partial x_i} - \frac{\partial\tau_{ij}}{\partial x_j}. \tag{2.7}$$

As in the case of Reynolds averaging, there is a closure problem, but in this case for the sub-grid scale Reynolds stresses. As in the case of RANS models, the eddy viscosity hypothesis can be used to relate the Reynolds stresses to the resolved rate of strain, $\overline{S_{ij}}$:

$$\tau_{ij}^r = -2\nu_t\overline{S_{ij}} + \frac{2}{3}k\delta_{ij}. \tag{2.8}$$

To close the problem, an implementation of the constant coefficient Smagorinsky model is used:

$$k = C_k \Delta^2 (S_{ij} S_{ij}); C_k = 0.202, \tag{2.9}$$

$$\nu_t = C_s \Delta^2 (S_{ij} S_{ij})^{1/2}; C_s = 0.02. \tag{2.10}$$

Finally, StarCD uses an *ad hoc* implementation of the filter width, Δ, that incorporates a simple wall damping function:

$$\Delta = V^{1/3}; \Delta_c = min(0.042y, \Delta), \tag{2.11}$$

where Δ_c is the filter width used in the solver and y is the distance to the nearest wall. It can be seen that at the wall ($y = 0$) this relationship gives a zero eddy viscosity. Although this is a crude wall function, the StarCD documentation recommends that the near-wall region be fully resolved, with the first cell having a distance less than $y^+ = 1$ and at least 30 cells in the boundary layer, which severely restricts the range of Reynolds numbers that can be accurately modeled using the LES approach (cd adapco 2005).

2.2. *Governing equations for particle/droplet motion*

The particle or droplet motion and breakup are calculated in the Lagrangian frame of reference. This approach requires interpolation of the surrounding carrier fluid velocity onto the center-of-mass of the computational particle representing the droplet. As is common practice in commerical CFD codes, StarCD uses a "parcel" approach in which each particle represents a collection of droplets with a fixed mass. If the droplets are broken or coalesce, the number of parcels *does not change*; instead the number of droplets represented by the parcel is modified. Parcel approaches keep the number of particles required to simulate the droplet physics manageable as explicit simulation of the millions of droplets present in even modest atomization problems is not possible. However, parcel approaches also underestimate the resulting dispersion of a particle or spray cloud. Lacking a better means of addressing this shortcoming, we used as large a number of parcels as computationally manageable.

The particle motion in the Lagrangian frame of reference is described by:

$$m_d \frac{d\vec{U_d}}{dt} = \vec{F_d} + \vec{F_p} + \vec{F_{vm}} + \vec{F_b}. \tag{2.12}$$

The aerodynamic drag is proportional to the slip velocity of the particles (which are assumed to be perfectly spherical):

$$\vec{F_d} = \frac{1}{2} C_d \rho_p A_p |\vec{u} - \vec{u_p}| (\vec{u} - \vec{u_p}). \tag{2.13}$$

The effect of local pressure gradients on the particle or droplet motion is given by:

$$\vec{F_p} = -V_d \nabla p. \tag{2.14}$$

In this work, we have chosen to neglect the forces due to "virtual mass" (F_{vm}), which results from the work required to displace the carrier fluid displaced by the drop and buoyancy forces (F_b).

For the spray calculations in the tractor-trailer geometry case, StarCD's droplet physics models were employed. These models include empirical correlations for aerodynamic breakup, collisions with both other drops and surfaces, and coalescence. We have found that droplet breakup largely results from collisions with surfaces and this effect is modeled using the correlations of Bai *et al.* (2002) implemented in StarCD. The model includes a wide range of droplet-wall collision behaviors: sticking (dry walls only; we assume

Mode	modified Weber range
Rebound	$5 < We_d$
Spread	$5 < We_d < 1320La^{-0.18}$
Splash	$We_d > 1320La^{-0.18}$

TABLE 1. Droplet wall impingement regimes from Bai *et al.* (2002).

wetted walls in this work), spreading, rebounding and splashing. The two important non-dimensional numbers in the model are a modified Weber number using the *wall-normal* velocity magnitude, We_d, and the Laplace number,

$$La = \frac{\rho\sigma D}{\mu^2}, \tag{2.15}$$

which characterizes the ratio of inertial to surface tension forces in the droplet. Based on empirical fitting of experimental data, Bai *et al.* (2002) obtained the relationships in Table 1 as a function of modified Weber number. With the impact type determined, the post-impingement characteristics are obtained. For the stick or spread modes, the droplets adhere to the wall; for the latter, the tangential velocity relative to the wall is modified. For a rebound collision, both the normal and tangential velocities are multiplied by an empirical restitution coefficient (which is negative in the case of the wall-normal velocity component) dependent on the incidence angle of the incoming droplet velocity to the wall. In the case of splash, new computational particles are created (breakup events typically do not lead to this outcome in StarCD's parcel methodology). Two daughter droplets are created and some portion of the original drop remains attached to the wall. The daughter or secondary parcels represent an equal amount of mass, with the total mass of both determined by an empirical, randomly specified ratio of the total secondary to incident droplet mass ratio:

$$r_s = 0.2 + 0.9X_r, \tag{2.16}$$

where X_r is a uniform deviate random number between 0 and 1. Note that the total secondary mass can actually exceed the incident droplet mass since the wall is assumed to be wetted and the daughter droplets can entrain some of the water film. The mass of the fluid remaining on the wall is $(1 - r_s)m_d$, where m_d is the mass of the incident droplet (parcel).

3. Problem Definition

3.1. *Plane Wake: Geometry*

The first case considered was a three-dimensional plane wake. This case was chosen since it clearly illustrates the phenomenon of "particle focusing" as discussed in Tang *et al.* (1992); Yang *et al.* (2000) and Luo *et al.* (2004). As there is some variation in the Reynolds numbers and geometric definitions in the aforementioned references, we have chosen a representative geometry and flow parameters that allow qualitative comparison to published results.

The geometry with mesh along with a detail of the particle injection scheme are shown in Figure 1. The plane has a thickness of 2 cm, with the entrance region having a length

Diameter	Stokes number
6×10^{-7}	1.33×10^{-3}
1.9×10^{-6}	1.33×10^{-2}
6×10^{-6}	1.33×10^{-1}
1.9×10^{-5}	1.33
1×10^{-3}	3680

TABLE 2. Summary of particle properties for plane wake investigation. Note the Stokes number is calculated using the inverse of the shear rate at the inlet walls ($500s^{-1}$) as a flow timescale

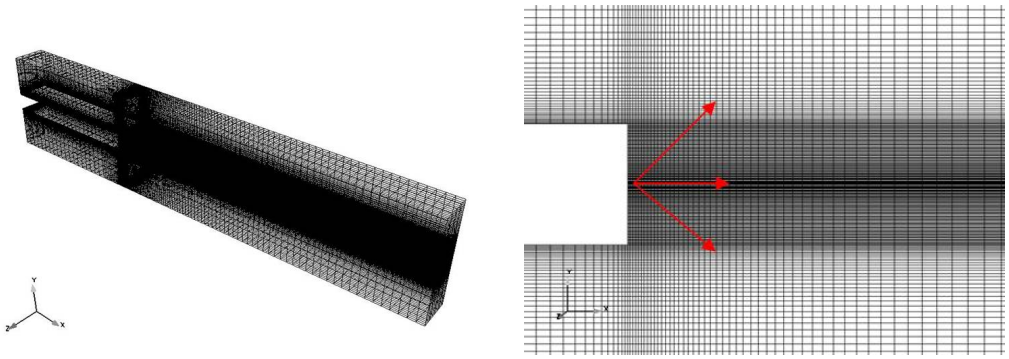

FIGURE 1. Mesh and domain used in plane wake simulations. Left: isometric view; Right: detail of near-plane region with particle injection vectors

of 18 cm and the wake region a length of 40 cm for a total domain length of 58 cm. The domain spanwise dimension is 4 cm and the the height above and below the plane is 10 cm for a total domain height of 12 cm. A block structured grid is used with dimensions of $20 \times 50 \times 5$ in the streamwise, wall-normal and spanwise directions respectively in the entrance region and a resolution of $237 \times 204 \times 5$ in the wake region. A hyperbolic tangent non-uniform grid spacing is used in the wall-normal direction such that the spacing of the first point off the wall is less than or approximately $y^+ = 1$. The mesh is clearly underresolved in the spanwise direction but allows some preliminary exploration of spanwise effects for the LES case. Also, no systematic investigation of the effect of the spanwise dimension on the wake characteristic was performed here.

Particles were injected at the point (0,0,2) at $\pm 45°$ and $0°$ with a velocity of 0.2 m/s and mass flowrate of 0.025 kg/s of each of the five particle sizes, defined in Table 2, giving a total mass injection rate of 0.125 kg/s. The particle density was fixed at 2400 g/m^3, equal to that of the glass beads used in the experimental studies of Tang *et al.* (1992) and Yang *et al.* (2000) and 200 parcels/second were injected for each size in each direction. Values of the Stokes number for each of the particle sizes in also provided in Table 2; a six order of magnitude variation in Stokes numbers was used to clearly illustrate inertial effects.

3.2. *Plane Wake: Simulation Parameters*

The flowrate was chosen such that the Reynolds number of the flow was 10000 based on the inlet channel mean velocity and plane width. A separate channel flow simulation

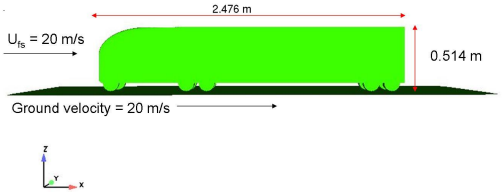

FIGURE 2. Schematic of GTS geometry and flow conditions

was used to generate fully developed inflow conditions using the same turbulence model employed in the wake simulation. Note that for the LES case, a lookup table containing the mean velocity and turbulent kinetic energy is used for the inlet boundary condition. In StarCD, the fluctuation velocity components are calculated from the turbulent kinetic energy by isotropically distributing the energy amongst the three components. A more rigorous procedure would use a time-dependent inflow database and read in instantaneous values of the mean and fluctuating velocity components. Based on DNS and LES studies of flat plate boundary layers (Lund *et al.* 1998; Na & Moin 1998; Rai & Moin 1993), we anticipate that the downstream flow will be strongly affected by the choice of inlet condition and that using isotropically distributed fluctuations will not give quantitatively correct flow behavior on the walls of the rectangular plane itself. However, since we are primarily interested in the qualitative differences in the wake structure and particle dispersion downstream of the plane these errors are expected to have minimal impact on the results presented here.

The simulation results showed a strong sensitivity to the choice of boundary conditions as well as domain size. Channel flow inlet regions with the length selected were used since using free boundaries in the inlet region resulted in strong pressure fluctuations that polluted the inlet profiles; using shorter inlet regions also gave this behavior. In the expansion region, it was necessary to use prescribed pressure boundaries on the three outlet surfaces with the pressure set to 0 Pa gauge pressure. Using the mass flow outlet condition in StarCD led to non-physical results and is not advised for multiple outlet faces. Cyclic boundary conditions were used in the spanwise direction.

The simulations were first completed using steady RANS to generate a starting flow field. The simulations were then run for approximately one flow through time using unsteady RANS or LES to generate the time-dependent flow field. Despite the symmetric mesh, it was not necessary to artificially perturb the flow field to set up the vortex street in the wake. The resulting time dependent flow field was used for the particle dispersion calculations. The total time of the dispersion calculations was 0.1 sec, using a timestep of 5×10^{-5} sec ($CFL \approx 0.5$).

3.3. *Simplified heavy vehicle (GTS): Geometry*

For the second part of this study, we considered a simplified heavy vehicle geometry: a modified version of the Ground Transportation System or GTS. Unlike the GTS model used in previous experimental (Croll *et al.* 1996; Storms *et al.* 2001) and computational (Salari *et al.* 2004) studies, this model includes wheels; a schematic of the geometry is shown in Figure 2. For this study we have used GTS model dimensions corresponding to those of a 1/8-scale wind tunnel model.

The computational domain was meshed using the commerical meshing program Harpoon, which generates body-fitted hexahedral dominant unstructured meshes. The settings for the Harpoon mesh generation are provided in Table 3; the mesh has approximately 2 million cells. The mesh was generated without hanging node transitions between

Parameter	Setting
Streamwise domain size (m)	14.95
Spanwise domain size (m)	4.5
Vertical domain size (m)	2.93
Base cell level (mm)	85
Refinement Box (x,y,z,level)	(-85:275;-60:60;-50:90),85 (+0)
Refinement Box (x,y,z,level)	(26:95;-35:35;-48:42),85 (+0)
Boundary layer total thickness (mm)	1
Boundary layer cell layers	3

TABLE 3. Mesh generation settings used in Harpoon for GTS model. Note that Harpoon's adaptive surface resolution tool was used with both the Gaussian curvature and proximity options enabled.

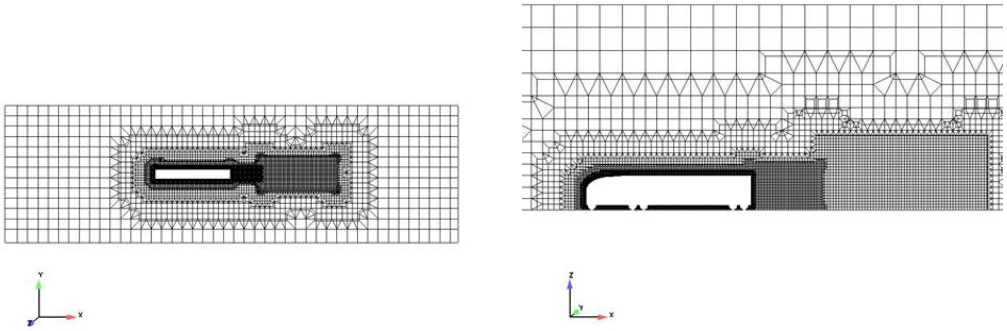

FIGURE 3. Harpoon-generated GTS mesh. Left: top view; Right: side view

hexahedral cells of differing sizes to make the mesh portable to other research codes at LLNL. Illustrations of the mesh are provided in Figures 3 and 4. As shown in the figures, additional refinement regions were utilized along the front corners and in the wake to provide adequate resolution of these regions of strong spatial velocity variation. The GTS is put in contact with the ground plane. Harpoon generates ground contact by extruding a small contact sleeve between the object and the ground plane as shown in Figure 4. The boundary layer extrusion was chosen such that the height of the first cell off the wall was in the range $10 < y^+ < 100$ which was adequate for the standard wall function approach used in the URANS calculations. For the LES calculations, this resolution is *not* sufficient as StarCD recommends a fully wall-resolved mesh with $y^+ < 1$ and at least 30 points in the boundary layer (cd adapco 2005). A discussion of near wall resolution and the use of wall functions can be found in Wilcox (2002), Durbin & Reif (2003) and Pope (2000). Note that for this preliminary, qualitative study only one mesh was used and that a grid resolution study is required to obtain quantitatively meaningful results.

3.4. *Tractor-Trailer (GTS): Simulation Parameters*

The simulations were performed using a free-stream velocity of 92 m/s, giving a width-based Reynolds number of approximately 2×10^6 corresponding to the value used in Salari *et al.* (2004). A moving ground plane with a velocity equal to that of the free stream is used. Note that the "wheels" are not rotating, so the contact regions between

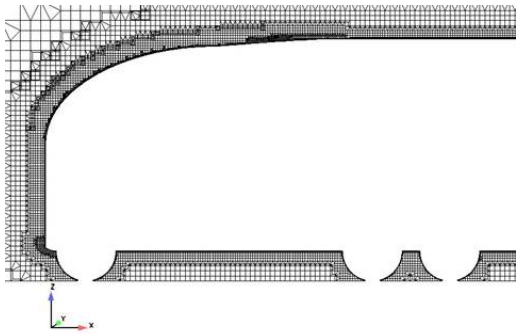

FIGURE 4. Detail of GTS mesh near front edges

the GTS and ground plane generate artificial flow features that would not be observed in a real-world wind tunnel test. However, this artifact of the problem definition is useful for illustrating the differences in the LES and URANS flowfield predictions as well as the resulting dispersion behavior; we will show the vortex structures resulting from the non-physical contact region are a strong function of the turbulence model (LES or URANS).

The water droplets were injected at the front of the wheel/body intersection at all of the wheels perpendicular to the free stream flow as well as at a 45° to the ground plane at the back edge of the contact plane of each wheel. Water droplets having diameters 1×10^{-5},1×10^{-4}, and 1×10^{-3} m were considered. The droplets were assumed to be water with a density 1000 kg/m^3 and surface tension of 72 dynes/cm. At each injection point, 250 parcels/sec with mass flowrate of 0.1 kg/s and velocity of 20 m/s were used for each droplet size. The choice of droplet injection velocity and direction is somewhat arbitrary. The values used here were chosen such that the differences in the resulting plume were easy to quantify. A more rigorous study would choose injection parameters based on available experimental measurements.

As in the case of the plane wake, the simulations were initialized using a steady RANS simulation then continued in a time-dependent manner with either the URANS or LES models. The time unsteady calculations were run for approximately 1000 timesteps before introduction of the spray. The spray simulations used a timestep of 5×10^{-5} seconds, giving a maximum CFL number of approximately 1, and were run for a total of 0.08 seconds.

4. Results and Discussion

4.1. *Dispersion in Plane Wake*

We begin by considering the differences in the flow fields predicted using the URANS and LES turbulence models for the plane wake. It should be emphasized that the simulations are underresolved in the spanwise direction and therefore the results should be taken as preliminary. The time-averaged mean velocity profiles in the wake are presented in Figure 5 and were obtained using averages of 20-point query lines in the post-processing program Ensight (CEI 2005). The differences are modest, with the LES and URANS predictions for both streamwise and spanwise velocity differing more strongly further downstream of the wake (x/H=0). The streamwise velocity profile far downstream of the plane is counterintuitive as the velocity defect region becomes a region of local acceleration; the origin of this effect is unclear but is probably an artifact of the outlet conditions. Despite

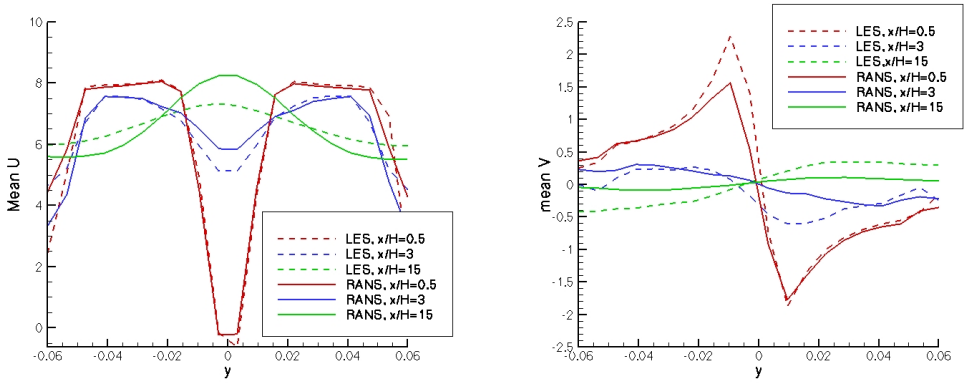

FIGURE 5. (Color) Time-averaged mean velocity profiles for plane wake as function of streamwise position. Left: streamwise velocity (U); Right: wall-normal velocity (V)

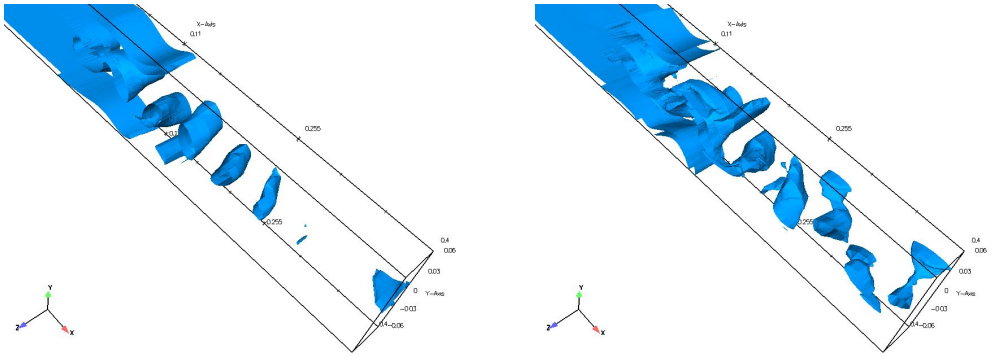

FIGURE 6. Comparison of vorticity isosurfaces at time=0.1 sec with equal threshold, Left: URANS; Right: LES

this anomaly, the results suggest the wake predicted using LES is more persistent and the instantaneous visualizations of vorticity magnitude isosurfaces presented in Figure 6 show that this is the case. The LES result shows more persistent roller structures all the way to the exit plane as well as a more complex and finer-scale structure near the wake. We anticipate that this finer structure will lead to different particle dispersion behavior in both the wall-normal and spanwise directions.

As shown in the instantaneous visualization in Figure 7, this is indeed the case. The particles in the RANS case show a stronger segregation due to the absence of the small recirculation regions visible in the vorticity contours in the LES case. The RANS case shows a clear segregation by Stokes number; small Stokes number particles are focused in the vortex cores, moderate Stokes number particles along the vortex edges and the largest behaving nearly ballistically. The LES case, having less coherent vortex structures in the wake, shows greater dispersion for all sizes of particles, particularly near the exit of the domain. These results are qualitatively similar to those presented in Tang *et al.* (1992); Yang *et al.* (2000); Luo *et al.* (2004) but because of the differences in boundary conditions and geometry it is not possible to make quantitative comparisons.

These differences in dispersion are quantified in Figure 8. The dispersion index is

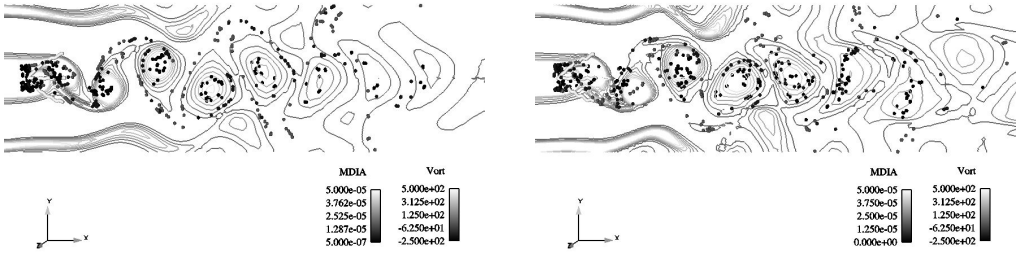

FIGURE 7. Comparison of vorticity contours and particle positions at time=0.1 sec. Left: URANS; Right: LES. Note stronger dispersion of small (dark) particles in LES case and preferential concentration of moderate sized particles in both cases along periphery of vortex regions

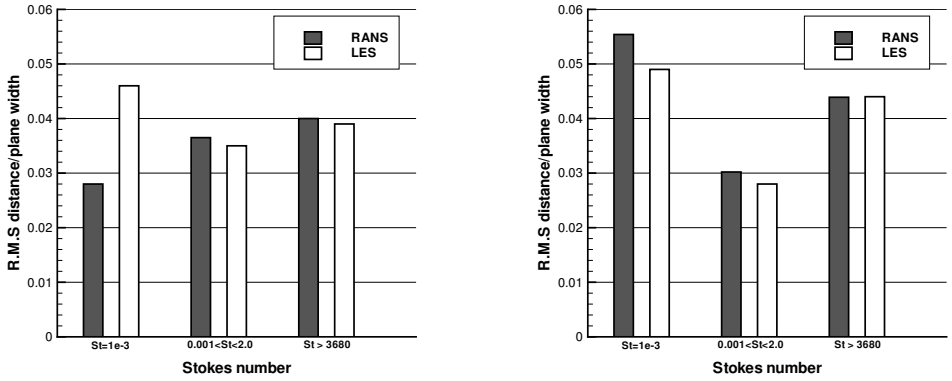

FIGURE 8. Instantaneous value of r.m.s. dispersion for plane wake normalized by the plane thickness. Left: dispersion in y-direction; Right: dispersion in z-direction

defined as:

$$D = \left(\frac{\sum_1^N (x_i - x_{i,0})^2}{N} \right)^{1/2}, \tag{4.1}$$

which is the r.m.s of the displacement of the particles from the injection point ($x_{i,0}$). For this analysis the displacements are normalized by the plane width (2 cm) and the plotted results are calculated using the particle displacements at t=0.1 sec. As expected from the visualization, the vertical dispersion is clearly larger ($\approx 40\%$) for the LES case. Somewhat less intuitively, the spanwise dispersion is actually lower in the LES case. Given the low spanwise resolution it is difficult to attribute great significance to this result and further study is needed. Overall, the higher Stokes number particles ($St > 0.001$) exhibit minor differences as the smaller structures in the flow do not strongly interact with them. This result has some interesting implications for the calculation of particle dispersion in bluff body wakes. If the particles of interest are sufficiently small ($St < 0.001$), URANS may strongly underpredict the dispersion; alternatively, if the particles of interest have even modest inertia ($St > 0.001$), URANS may be sufficient for dispersion estimates. Given the substantial computational demands of a properly resolved LES simulation, this may be a major simplification for some problems.

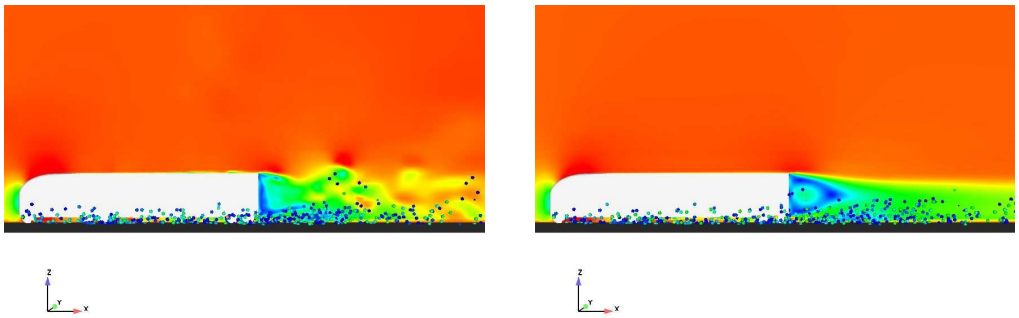

FIGURE 9. (Color) Instantaneous flow visualization of velocity magnitude along centerline with spray for GTS. Left: LES; Right: URANS. Note greater unsteadiness in the LES case as well as the increased vertical dispersion.

4.2. *Dispersion in tractor-trailer wake*

As might be expected from the plane wake results, the simulations using the GTS geometry also show substantial differences in both the flow field and particle dispersion calculations. The instantaneous visualizations shown in Figure 9 show qualitative differences in both the flow field and particle positions. The GTS wake is clearly much less structured in the LES case and the corresponding small-scale structures act to more strongly disperse the smallest droplets in both the vertical and spanwise (not obvious from the visualization) directions. The URANS wake structure is qualitatively similar to the results observed in the work of Salari *et al.* (2004) which did not use a moving ground plane.

The differences in the dispersion are again quantified using the dispersion index defined in Eq. 4.1. In this case, the dispersion index is presented in dimensional units. Since most of the droplets ultimately land on the moving ground plane but are still tracked by the solver, we only consider droplets in a sampling box slightly above the ground plane. As shown in Fig. 10, the results are qualitatively similar to those for the plane wake. The largest differences in dispersion are observed for the smallest particles ($d < 5 \times 10^{-5}$m). These droplets interact strongly with the smaller scale turbulent structures captured using the LES model. Larger droplets exhibit modest variation in dispersion index between the two turbulence models as they interact much more weakly with the aforementioned flow structures. These results suggest that LES is necessary to accurately predict the dispersion of small, low-inertia droplets.

5. Conclusions and Recommendations

The dispersion of particles or droplets in two bluff body wakes has been modeled using the commercial CFD code StarCD using the unsteady RANS and LES turbulence models. In the case of the plane wake, "particle focusing" was observed in agreement with published data. In both cases, the flow fields predicted using LES exhibited smaller-scale coherent structures than observed in the URANS calculations. These small-scale flow structures interacted strongly with the lowest inertia particles giving rise to large differences in dispersion. Larger particles having greater inertia did not interact with these flow features and the resulting dispersion profiles were largely similar between the two models. In the case of the plane wake, the threshold for this difference in behavior was $St = 0.001$, but the exact value depends on the Reynolds number and characteristic flow

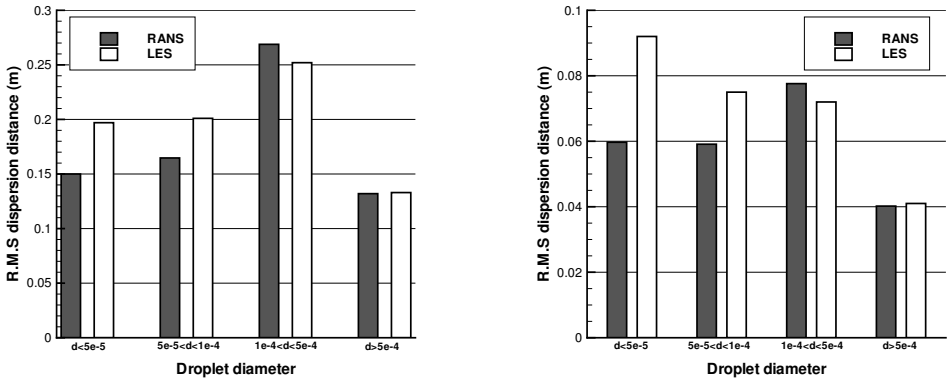

FIGURE 10. Instantaneous value of r.m.s. dispersion for GTS. Left: dispersion in y-direction (wall-normal); Right: dispersion in z-direction (spanwise)

time scale of the problem of interest. The characteristic flow time scale is often difficult to estimate and it is expected that some computational scoping studies would be necessary for a given problem. Regardless, the implication is that LES may be unnecessary (and URANS adequate) for problems involving dispersion of moderate inertia particles. Use of URANS may make numerical investigation of these problems considerably easier.

In the case of spray, this conclusion may not be as generally applicable as both dispersion and breakup are important. As shown in the study of Apte *et al.* (2003), in cases for which aerodynamic breakup is important, the use of LES may be considerably more accurate than RANS in predicting the resulting size distribution. This metric was not considered in this study given the lack of experimental data with which to compare. LES models also allow the implementation of more sophisticated breakup models than those currently implemented in StarCD. This aspect of LES simulation should be investigated in future studies.

Finally, we note that we have made the implicit assumption that the LES results obtained here are inherently more accurate than those obtained using URANS. This assumption may not necessarily be true. A detailed quantitative benchmarking of the results obtained using the URANS and LES model in StarCD on a properly resolved mesh should be performed on a "canonical" external problem such as the $Re = 3900$ flow around a cylinder. An investigation of this type would provide a more accurate assessment of the quality of the LES implementation in and solutions obtained with StarCD.

6. Acknowledgments

This work was performed under the auspices of the U.S. Department of Energy by the University of California, Lawrence Livermore National Laboratory under Contract No. W-7405-ENG-48. Helpful discussions with Kambiz Salari, Jason Ortega, Paul Castellucci and Craig Eastwood are gratefully acknowledged. Portions of this work were presented at the 6th Biennial Tri-Laboratory Engineering Conference, Monterey, CA, in Sep. 2005 and the Society of Automotive Engineers Commercial Vehicle Exposition, Chicago, IL, in Nov. 2005.

REFERENCES

CD ADAPCO 2005 StarCD v.3.24, http://www.cd-adapco.com/products/STARCD/index.html.

APTE, S., MAHESH, K., MOIN, P. & OEFELEIN, J. 2003 Large-eddy simulation of swirling particle-laden flows in a coaxial-jet combustor. *Intl. J. Multiphase Flow* **29**, 1311–1331.

BAI, C., RUSCHE, H. & GOSMAN, A. 2002 Modeling of gasoline spray impingment. *Atomization and Sprays* **12**, 1–27.

CEI 2005 Ensight v.8.07, http://www.ensight.com/products/ensight.html.

CROLL, R., GUTIERREZ, W., HASSAN, B., SUAZO, J. & RIGGINS, A. 1996 Experimental investigation of the ground transportation systems (gts) project for heavy vehicle drag reduction. *Tech. Rep.* 960907. SAE.

DURBIN, P. & REIF, B. P. 2003 *Statistical Theory and Modeling for turbulent flows*. Wiley.

EATON, J. & FESSLER, J. 1994 Preferential concentration of particles by turbulence. *Intl. J. Multiphase Flow* **20S**, 169–209.

IACCARINO, G. 2001 Predictions of a turbulent separated flow using commercial cfd codes. *ASME J. Fluids Eng.* **123**, 819–828.

IACCARINO, G., OOI, A., DURBIN, P. & BEHNIA, M. 2003 Reynolds averaged simulation of unsteady separated flow. *Intl. J. of Heat and Fluid Flow* pp. 147–156.

KRISHNAN, V., SQUIRES, K. & FORSYTHE, J. 2004 Prediction of separated flow characteristics over a hump using RANS and DES. *Tech. Rep.*. AIAA-2004-2224.

LUND, T., WU, X. & SQUIRES, K. 1998 Generation of turbulent inflow data for spatially-developing boundary layer simulations. *J. Comp. Phys.* **140**, 233–258.

LUO, K., FAN, J., JIN, H. & CEN, K. 2004 Les of the turbulent coherent structures and particle dispersion in the gas-solid wake flows. *Powder Tech.* **147**, 49–58.

MANSER, M., KOPPA, R. & MOUSLEY, P. 2003 Evaluation of splash and spray suppression devices on large trucks during wet weather. *Tech. Rep.*. AAA Foundation for Traffic Safety, www.aaafoundation.org.

MENTER, F. 1994 Two-equation eddy-viscosity turbulence models for engineering applications. *AIAA J.* **32**, 1598–1605.

NA, Y. & MOIN, P. 1998 Direct numerical simulation of a separated turbulent boundary layer. *J. Fluid Mech.* **374**, 175–201.

POPE, S. 2000 *Turbulent Flows*. Cambridge Univ. Press.

RAI, M. & MOIN, P. 1993 Direct numerical simulation of transition and turbulence in a spatially evolving turbulent boundary layer. *J. Comp. Phys.* **109** (2), 169–192.

RODI, W. 1997 Comparison of les and rans calculations of the flow around bluff bodies. *J. Wind Eng. and Ind. Aero.* **69–71**, 55–75.

SALARI, K., ORTEGA, J. & CASTELLUCCI, P. 2004 Computational prediction of aerodynamic forces for a simplified integrated tractor-trailer geometry. *Tech. Rep.*. AIAA-2004-2253.

SOMMERFELD, M. & QIU, H.-H. 1993 Characterization of particle-laden, confined swirling flows by phase-doppler anemometry and numerical calculation. *Intl. J. Multiphase Flow* **19**, 1093–1127.

STORMS, B., ROSS, J., HEINECK, J., WALKER, S., DRIVER, D., ZILLIAC, G. & BENCZE, D. 2001 An experimental study of the ground transportation system (GTS) model in the NASA ames 7-by-10-ft wind tunnel. *Tech. Rep.*. NASA/TM-2001-209621.

TANG, L., WEN, F., YANG, Y., CROWE, C., CHUNG, J. & TROUTT, T. 1992 Self-organizing particle dispersion mechanism in a plane wake. *Phys. Fluids A* **4** (10), 2244–2251.

WILCOX, D. 2002 *Turbulence Modeling for CFD*. DCW Industries.

YANG, Y., CROWE, C., CHUNG, J. & TROUTT, T. 2000 Experiments on particle dispersion in a plane wake. *Intl. J. Multiphase Flow* **26**, 1583–1607.